Available online at www.sciencedirect.com
SCIENCE DIRECT®
International Journal of Heat and Mass Transfer 48 (2005) 561–572
International Journal of HEAT and MASS TRANSFER
www.elsevier.com/locate/ijhmt

Numerical simulation of conjugate heat and mass transfer process within cylindrical porous media with cylindrical dielectric cores in microwave freeze-drying

Zhi Tao [a,*], Hongwei Wu [a,b,1], Guohua Chen [b,2], Hongwu Deng [a,1]

[a] National Laboratory on Aero-engines, School of Jet Propulsion, Beijing University of Aeronautics and Astronautics, Beijing, China
[b] Department of Chemical Engineering, The Hong Kong University of Science and Technology, Clear Water Bay, Kowloon, Hong Kong, China

Received 26 June 2003; received in revised form 10 September 2004

Abstract

This paper presents a numerical model for the process of microwave freeze-drying within a cylindrical porous media with cylindrical dielectric cores. The set of transient governing equations developed are solved numerically with variable time-step finite volume method. Analysis of numerical results may lead to following main conclusions for the new freeze-drying process: (1) Proper usage of cylindrical dielectric cores could dramatically reduce the drying time. (2) The loss factor ε'' of the cylindrical dielectric core is an important parameter influencing the drying behavior. (3) Two sublimation fronts do exist within the porous media due to the existence of inner dielectric cores. (4) The impact of cylindrical dielectric cores on drying could not be ignored even though the initial saturation is low ($S_0 = 0.2$).

Keywords: Heat and mass transfer; Freeze-drying; Porous media; Cylindrical dielectric core; Loss factor

1. Introduction

Freeze-drying (lyophilization) is used as a gentle dehydration method for heat sensitive materials especially in food and pharmaceutical industries, usually for the purpose of preservation. It is well known for its ability to sustain the high quality of products (colour, shape, aroma, texture, biological activity, etc.) than any other drying methods due to its low processing temperature and no oxygen involved in the process. Other advantages of freeze-drying include its protection against chemical decomposition, ease of rehydration, etc. However, freeze-drying is an expensive dehydration process because of low drying rates, high capital and energy costs generated by refrigeration and vacuum systems, and relatively long drying time required [1–5]. As a consequence, the use of freeze-drying on the industrial scale is restricted to high added-value products. Freeze-drying by microwave heating, however, has proven to overcome those disadvantages as it has the characteristic

* Corresponding author. Tel.: +86 10 8231 7443; fax: +86 10 8231 7432.
E-mail addresses: tao_zhi@buaa.edu.cn (Z. Tao), hongwei_wu@hotmail.com (H. Wu), kechengh@ust.hk (G. Chen), deng.yy@263.net (H. Deng).
[1] Tel.: +86 10 8231 4545.
[2] Tel.: +852 2358 7138; fax: +852 2358 0054.

0017-9310/$ - see front matter © 2004 Elsevier Ltd. All rights reserved.
doi:10.1016/j.ijheatmasstransfer.2004.09.008

Nomenclature

a	coefficient
A	area, m^2
b	source term
c	specific heat, J/(kg °C)
D	diffusivity, m^2/s
E	electric field strength, V/m
f	frequency, MHz
ΔH	sublimation latent heat of ice, J/kg
I	vapor source intensity, $kg/(m^3 s)$
J	mass flux, $kg/(m^2 s)$
J_{vs}	mass flux of vapor in icy region, $kg/(m^2 s)$
K_D	permeability, m^2
K_r	relative permeability,
m	mass, kg
P	pressure, Pa
P_R	vacuum pressure, Pa
q	density of microwave power absorbed, $J/(s m^3)$
r	polar coordinate direction
R	water vapor gas constant, $m^2/(s^2 K)$
R_d	radius of cylindrical dielectric core, m
R_P	initial radius of porous material, m
S	saturation (ice volume)/(void volume)
t	temperature, °C
T	temperature, K
T_R	vacuum temperature, K
u	velocity, m/s
u_{sat}	moisture content, $kg/(m^3)$
V	volume, m^3

Greek symbols

α	heat transfer coefficient, $W/(m^2 °C)$
ε	porosity
ε'	permittivity, F/m
ε''	loss factor
ϕ	generalized variable
λ	thermal conductivity, W/(m °C)
μ	viscosity, kg/(m s)
ρ	density, kg/m^3
τ	time, s
ξ	small value

Subscripts

0	initial
1	first sublimation front
2	second sublimation front
a	with cylindrical dielectric core
b	without cylindrical dielectric core
d	cylindrical dielectric core
e	effective
f	sublimation front
F	final time
i	ice
I	initial time
nb	neighbor
p	current control volume
s	solid body
v	vapor
w	wall of porous material

of heating up materials volumetrically. Experiments and numerical predictions all showed that the microwave freeze-drying appears to be one of the most promising techniques to accelerate the rate of dehydration and enhance overall quality [6–14].

Copson, in 1962, firstly modeled the microwave freeze-drying process with pseudo steady- state assumption that had been used in conventional freeze-drying modeling. Much efforts have been devoted afterwards to this area by many researchers [7,15,10,11,16,17]. Ma and Peltre [18] presented a transient one-dimensional model, which was the first transient analysis of microwave freeze-drying. A more general analysis was undertaken by Ma and Peltre [10,11] to improve the accuracy of the Copson model, and was later extended to be two-dimensional by Ang et al. [12] to take into account of the material anisotropy. Chen et al. [19] studied volatile retention in microwave freeze dried model foods. Wang and Shi [20–24] developed a model which took into account the sublimation or condensation by vapor transport in the unsaturated frozen region, and saturation change was considered. Further research on microwave freeze-drying focused on optimization of combined radiant and microwave aided freeze-drying [17] and solid entrainment [25,26].

Although ordinary microwave freeze-drying could dramatically accelerate the drying process, it has much room to be enhanced further by adding dielectric cores to the porous materials to be dried. The dielectric core is functioning an another heat source because the dielectric core has to be properly selected high loss factor than ice so that the microwave energy will be mainly taken by the core during drying. In this way, the porous material will be heated from both inside and outside at the same time, which could remarkably increase the drying process. Adding dielectric cores is, therefore, a novel, interesting, and also industrially relevant drying technique. Wu et al. [27] presented a double sublimation front model within spherical porous media with dielectric cores in microwave freeze-drying. By now, there is not a single report on using dielectric materials within cylindrical porous media in microwave freeze-drying.

In the present study, a numerical simulation is carried out to investigate the microwave freeze-drying with

cylindrical dielectric cores. A transient model is developed and it has three sets of governing equations for the dried, the icy and the dielectric regions, respectively. Since these regions are coupled together by energy and mass transfer, the corresponding three sets of equations have to be solved simultaneously. This complex conjugate problem is tackled with variable time-step finite volume method. The main objective of this study is to see the feasibility of microwave freeze-drying with cylindrical dielectric cores and any new phenomena pertinent.

2. Mathematical modeling

The simplified one-dimensional physical configuration for the present model is illustrated in Fig. 1. As for the porous media with the cylindrical dielectric core in microwave freeze-drying, because the porous material is heated from both inside and outside, there may exist two sublimation fronts, as demonstrated previously [27]. Ice in the outer layer of material absorbs microwave heating energy and sublimates, which forms the first sublimation front. On the other hand, since the dielectric materials has higher loss factor than that of ice, the microwave energy will be mainly taken by dielectric materials and then conducted to the porous layer, and this energy will vaporize the ice and the second sublimation front is so formed. Vapor sublimated in this region will be convected through voids to the outside. An intriguing corollary is that, four distinct regions within the cylindrical porous media are discernible: the two dried regions, the icy region, and the cylindrical dielectric core, as indicated in Fig. 1.

The following assumptions are often made to simplify the governing equations:

(i) Only water vapor is in the vacuum chamber and ideal gas law is applicable. Inert gases dissolved in the product are not considered.
(ii) Local thermodynamic equilibrium is assumed.
(iii) The porous media are homogeneous and isotropical, and the structure of the porous material is considered to be rigid and unaltered with time.
(iv) The incident electric field is assumed uniform in the material.
(v) Sublimation occurs at an interface parallel to the surface of the porous materials to be dried, and the thickness of the interface is infinitesimal [28–30].

Other simplifications are described in the due course.

Based on the above assumptions, the set of governing equations for each of the distinct regions are as follows.

2.1. Governing equations

2.1.1. Dried region

Mass conservation

Mass conservation in cylindrical coordinates form is

$$\frac{\partial(\varepsilon\rho_v)}{\partial\tau} = \frac{1}{r}\frac{\partial(r\cdot J_v)}{\partial r} \tag{1}$$

$$J_v = D_e\frac{\partial\rho_v}{\partial r} - \varepsilon\rho_v u_v \tag{2}$$

where J_v is the total mass flux in dried region, $D_e\frac{\partial\rho_v}{\partial r}$ is diffusion term and $\varepsilon\rho_v u_v$ is convection term. If the convection term in the material is negligible, as is always the case, the mass transfer in the dried region can be written as

$$\frac{\partial(\varepsilon\rho_v)}{\partial\tau} = \frac{1}{r}\frac{\partial\left(r\cdot D_e\frac{\partial\rho_v}{\partial r}\right)}{\partial r} \tag{3}$$

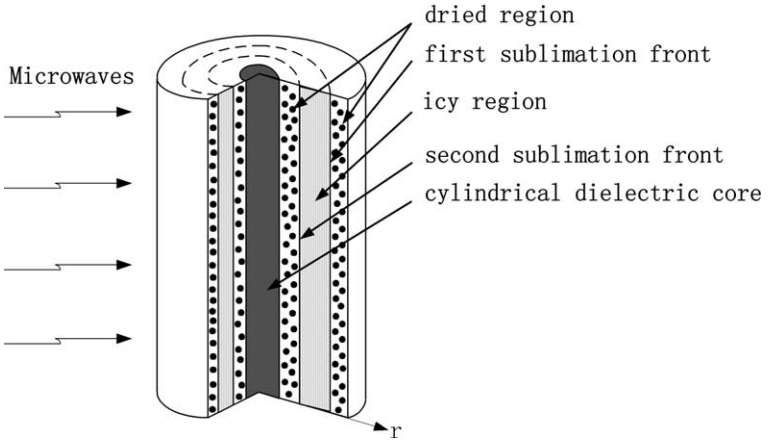

Fig. 1. Schematic of microwave freeze-drying with the cylindrical dielectric core.

Energy conservation

The following is the cylindrical coordinates form:

$$\frac{\partial(\rho cT)}{\partial\tau}=\frac{1}{r}\frac{\partial\left(r\cdot\lambda\frac{\partial T}{\partial r}\right)}{\partial r}+q \tag{4}$$

By volume averaging [31], the following is obtained:

$$\rho c=\rho_s c_s(1-\varepsilon)+\rho_v c_v\varepsilon \tag{5}$$

$$\lambda=\lambda_s(1-\varepsilon)+\lambda_v\varepsilon \tag{6}$$

2.1.2. Icy region

The vapor continuity equation

$$\frac{\partial}{\partial\tau}[(1-S)\varepsilon\rho_v]=-\frac{1}{r}\frac{\partial(r\cdot J_{vs})}{\partial r}+I \tag{7}$$

$$I=-\frac{\partial(\varepsilon S\rho_i)}{\partial\tau} \tag{8}$$

where S is the ice volume fraction in icy region, J_{vs} is the mass flux of vapor in icy region and I is the vapor source intensity.

Based on the Darcy's law and Fick's law, vapor flow in this region can be expressed as

$$J_{vs}=-\frac{K_D K_r}{\mu_v}\rho_v\frac{\partial P_v}{\partial r}-(1-S)\varepsilon D\frac{\partial\rho_v}{\partial r} \tag{9}$$

According to $P_v=\rho_v RT$, Eq. (9) becomes

$$\begin{aligned}J_{vs}&=-\frac{K_D K_r}{\mu_v}\rho_v\frac{\partial(\rho_v RT)}{\partial r}-(1-S)\varepsilon D\frac{\partial\rho_v}{\partial r}\\&=-K\frac{\partial T}{\partial r}\end{aligned} \tag{10}$$

where

$$K=\frac{K_D K_r}{\mu_v}R\rho_v^2+\left[\frac{K_D K_r}{\mu_v}R\rho_v T+(1-S)\varepsilon D\right]\times\frac{\partial\rho_v}{\partial T} \tag{11}$$

Substituting Eq. (10) into Eq. (7) leads to

$$(1-S)\varepsilon\frac{d\rho_v}{dT}\frac{\partial T}{\partial\tau}-\varepsilon\rho_v\frac{\partial S}{\partial\tau}=\frac{\partial}{\partial r}\left(K\frac{\partial T}{\partial r}\right)+I \tag{12}$$

Based on the fact that

$$\rho_i\gg\rho_v \tag{13}$$

The following equation can be derived:

$$I=-\frac{\partial}{\partial r}\left(K\frac{\partial T}{\partial r}\right)+(1-S)\varepsilon\frac{d\rho_v}{dT}\frac{\partial T}{\partial\tau} \tag{14}$$

Energy conservation

Neglecting the heat transfer caused by vapor convection, the energy balance equation in icy region can be written as

$$\frac{\partial(\rho cT)}{\partial\tau}=\frac{1}{r}\frac{\partial\left(r\cdot\lambda\frac{\partial T}{\partial r}\right)}{\partial r}-I\cdot\Delta H+q-\frac{\partial}{\partial r}(c_v TJ_{vs}) \tag{15}$$

According to volume averaging, the following are given by Eqs. (16) and (17), respectively:

$$\rho c=\rho_s c_s(1-\varepsilon)+\rho_i c_i\varepsilon S+\rho_v c_v\varepsilon(1-S) \tag{16}$$

$$\lambda=\lambda_s(1-\varepsilon)+\lambda_i\varepsilon S+\lambda_v\varepsilon(1-S) \tag{17}$$

Eq. (15) can be simplified by using Eq. (14) as follows:

$$\frac{\partial[(\rho c)_e T]}{\partial\tau}=\frac{1}{r}\frac{\partial\left(r\cdot\lambda_e\frac{\partial T}{\partial r}\right)}{\partial r}+q \tag{18}$$

where

$$\begin{aligned}(\rho c)_e&=\rho_s c_s(1-\varepsilon)+\rho_i c_i\varepsilon S+\rho_v c_v\varepsilon(1-S)\\&\quad+(1-S)\varepsilon\frac{d\rho_v}{dT}\cdot\Delta H\end{aligned} \tag{19}$$

$$\lambda_e=\lambda_s(1-\varepsilon)+\lambda_i\varepsilon S+\lambda_v\varepsilon(1-S)+K\cdot\Delta H+c_v TK \tag{20}$$

Combination of Eqs. (14) and (18) leads to

$$-u_{sat}\frac{\partial S}{\partial\tau}=-\frac{1}{r}\frac{\partial\left(r\cdot K\frac{\partial T}{\partial r}\right)}{\partial r}+f_t\frac{1}{r}\frac{\partial\left(r\cdot\lambda_e\frac{\partial T}{\partial r}\right)}{\partial r}+f_t q \tag{21}$$

where

$$f_t=\frac{\varepsilon(1-S)}{(\rho c)_e}\cdot\frac{d\rho_v}{dT} \tag{22}$$

2.1.3. Within the cylindrical dielectric core

Heat transfer

$$\frac{\partial(\rho_d c_d T)}{\partial\tau}=\frac{1}{r}\frac{\partial\left(r\cdot\lambda_d\frac{\partial T}{\partial r}\right)}{\partial r}+q_d \tag{23}$$

2.1.4. Sublimation fronts

For the first sublimation front, see Fig. 1

$$J_{vf1}=\left(-u_{sat}S\cdot\frac{\partial r}{\partial\tau}\right)\Big|_{r=r_1^-} \tag{24}$$

Mass conservation

$$\left(-D_e\cdot\frac{\partial\rho_v}{\partial r}\right)\Big|_{r=r_1^+}-\left(-K\cdot\frac{\partial T}{\partial r}\right)\Big|_{r=r_1^-}=J_{vf1} \tag{25}$$

Energy conservation

$$\left(-\lambda_e\cdot\frac{\partial T}{\partial r}\right)\Big|_{r=r_1^-}-\left(-\lambda\cdot\frac{\partial T}{\partial r}\right)\Big|_{r=r_1^+}=J_{vf1}\cdot\Delta H \tag{26}$$

For the second sublimation front, see Fig. 1

$$J_{vf2}=\left(u_{sat}S\cdot\frac{\partial r}{\partial\tau}\right)\Big|_{r=r_2^+} \tag{27}$$

Mass conservation

$$-\left(-D_e\cdot\frac{\partial\rho_v}{\partial r}\right)\Big|_{r=r_2^-}+\left(-K\cdot\frac{\partial T}{\partial r}\right)\Big|_{r=r_2^+}=J_{vf2} \tag{28}$$

Energy conservation

$$\left(-\lambda\cdot\frac{\partial T}{\partial r}\right)\Big|_{r=r_2^-}-\left(-\lambda_e\cdot\frac{\partial T}{\partial r}\right)\Big|_{r=r_2^+}=J_{vf2}\cdot\Delta H \tag{29}$$

2.1.5. Boundary conditions

Due to symmetry of the material, the boundary conditions at the center and surface are

$$-\lambda_d \cdot \left.\frac{\partial T}{\partial r}\right|_{r=0} = 0 \tag{30}$$

$$\left(-\lambda \cdot \frac{\partial T}{\partial r}\right)\Big|_{r=R_p} = \alpha(T|_{r=R_p} - T_R) \tag{31}$$

$$\rho_v|_{r=R_p} = \frac{P_R}{RT}_{r=R_P} \tag{32}$$

$$\left.\frac{\partial \rho_v}{\partial r}\right|_{r=0} = 0 \tag{33}$$

$$\left.\frac{\partial \rho_v}{\partial r}\right|_{r=r_d} = 0 \tag{34}$$

2.1.6. Initial conditions

$$T|_{\tau=0} = T_0 \tag{35}$$

$$R|_{\tau=0} = R_p \tag{36}$$

$$S|_{\tau=0} = S_0 \tag{37}$$

The microwave power dissipation per unit volume within the material is related to the electric field strength E and the dielectric properties of the material by the following equation $q = 2\pi f\varepsilon'\varepsilon'' E^2$.

2.1.7. General energy balance

$$Q_1 + Q_2 + Q_3 = Q_4 + Q_5 + Q_6 + Q_7 + Q_8 \tag{38}$$

where

$Q_1 = \int_{\tau_1}^{\tau_F} q_i V_i \,d\tau$ the quantity of microwave power that is absorbed by the ice during the whole drying

$Q_2 = q_d V_d \tau_F$ the quantity of microwave power that is absorbed by the cylindrical dielectric core during the whole drying

$Q_3 = q_s V_s \tau_F$ the quantity of microwave power that is absorbed by the material during the whole drying

$Q_4 = \int_{\tau_1}^{\tau_F} c_i m_i (T_i - T_0)\,d\tau$ the energy needed when ice converted into vapor at sublimation temperature during drying

$Q_5 = \int_{\tau_1}^{\tau_F} c_d m_d (T_d - T_0)\,d\tau$ the energy needed for the cylindrical dielectric core from the start to the end of the drying process

$Q_6 = \int_{\tau_1}^{\tau_F} c_s m_s (T_s - T_0)\,d\tau$ the energy needed for the material from beginning to the end of the drying process

$Q_7 = m_i \cdot \Delta H$ the energy needed for the sublimation of ice during the whole drying

$Q_8 = \int_{\tau_1}^{\tau_F} \alpha A_w (T_w - T_R)\,d\tau$ the transmitted energy flux at the surface of the material?

3. Physical properties

This research aims to investigate the phenomena of microwave freeze-drying of cylindrical porous media with cylindrical dielectric cores, and to further verify the applicability of the previously studied double sublimation front model developed for spherical porous media with spherical dielectric cores [27]. It is, therefore, reasonable not to limit to any specific materials, a set of commonly accepted physical properties are more favorable to reveal general inherent natures. The selected physical properties are listed in Table 1 and they are all selected from previously published references.

4. Numerical results

The computational domain shown in Fig. 2 was divided into a series of control volumes and Eqs. (1)–(23) were integrated within each volume. Take ϕ as the generalized variable for ρ, T and S, the governing equations of Eqs. (1)–(23) were discretized into a set of algebraic equations, with fully implicit scheme and variable time-steps, in the form of

$$a_p \phi_p = \sum a_{nb} \phi_{nb} + b \tag{39}$$

where a_p and a_{nb} are the coefficient matrix and b is the source term.

Eq. (39) was solved with tridiagonal matrix method (TDMA). At each time step, the solution is considered to have achieved convergence if

$$\left|\frac{\sum[\phi^{(n+1)} - \phi^{(n)}]}{L}\right| \leqslant \xi \tag{40}$$

For different variables ρ, T and S, the ξ would be 10^{-9}, 10^{-3} and 10^{-5}, respectively. It implied that a dimensionless variable was applied for the convergence criteria in the program. In order to reduce the error caused by the explicit format, a sufficiently fine grid was used. During the program, test solutions for a typical operation were obtained by utilizing different grid sizes to check the grid independence. It was found that the difference of drying time between the calculations of 550- and 600-grid is less than 0.1%. Thus the 550-grid was used in all computations.

In addition, comparison was done by calculating the drying times of two identical porous media with cylindrical dielectric cores. However, the first cylindrical dielectric core has normal properties while the second has a zero thermal conductivity and a zero loss factor. The second porous media could be taken as having no cylindrical dielectric core because it has no effects of any sorts on the drying process except taking up the same volume.

Table 2 lists the typical operating conditions employed in the simulation.

Table 1
Physical properties for the drying model

Symbol	Value or expressions	Unit	References
c_v	1866.0	J/(kg K)	[32]
c_s	1505.0	J/(kg K)	Assumed
c_i	2090.0	J/(kg K)	[33]
c_{die}	189.0	J/(kg K)	Assumed
λ_v	0.0022	W/(m °C)	[32]
λ_s	0.20	W/(m °C)	[10,11]
λ_i	2.22	W/(m °C)	[33]
λ_{die}	0.10	W/(m °C)	[32]
ρ_v	$0.1 \times \exp(-53.7881 + 0.294552 \times T - 3.987875 \times 10^{-4} T^2)$	kg/m^3	[33]
ρ_s	320.0	kg/m^3	[10,11]
ρ_i	913.0	kg/m^3	[33]
ρ_{die}	2500.0	kg/m^3	[32]
ΔH	2,821,500.0	J/kg	[33]
ε	0.7	Dimensionless	Assumed
D_e	$\frac{78.5 \times 10^{-4}}{(3.4 + p_v/133.3)}$	m^2/s	[10,11]
K_D	$4.44 \times 10^{-13} + 3.1589 \times 10^{-12} \times p_v$	m^2	[34]
K_r	1-S	Dimensionless	[21]

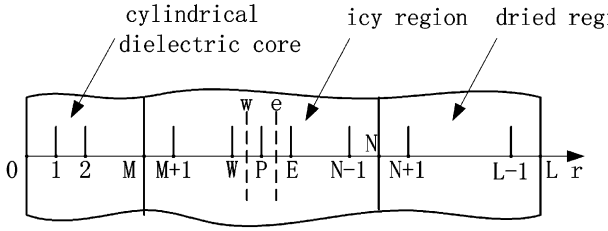

Fig. 2. Schematic drawing for discretization of governing equations.

Fig. 3(a) and (b) shows the calculated temperature and saturation distributions in the cylindrical porous material during microwave freeze-drying without a cylindrical dielectric core. The abscissa in Fig. 3 is the distance from the cavity which is 1.1 mm for the original, the same radius as the cylindrical dielectric core. The temperature and saturation profiles at different time, τ = 541, 1613, 2643, 3607, 4479, 5225 and 5790 s are shown and marked 1, 2, 3, 4, 5, 6 and 7, respectively. During the initial stage, the sublimation front is close to the surface of porous material as expected, lower transfer resistance and higher mass transfer driving force of vapor results in higher mass flux in the dried region. As the position of the sublimation front recedes, the mass transfer resistance increases. It should, therefore, be noted that the temperature of the sublimation front increases gradually, to maintain a high mass transfer driving force throughout the drying process, as shown in Fig. 3(a). The surface temperature of material is lower than that of environment at the start of drying. As a consequence, the heat will be absorbed by the material from the environment at this stage. Note also that the heat begins to flow out to the environment as the drying process proceeded. Moreover, it is observed that the maximum temperature in outer dried region will move from the surface to the inside of the material, according to the curves presented in Fig. 3(a). The saturation dis-

Table 2
Typical operating conditions

Symbol	Value	Unit
E	2500.0	V/m
f	2450.0	MHz
P_R	15.0	Pa
R_d	1.1	mm
R_p	7.0	mm
S_0	0.8	—
T_0	−15.0	°C
T_R	20.0	°C
α	10.0	W/(m^2 °C)
ε	0.75	–
ε''_d	6.0	–
ε''_i	0.003	–
ε''_s	1.0	–

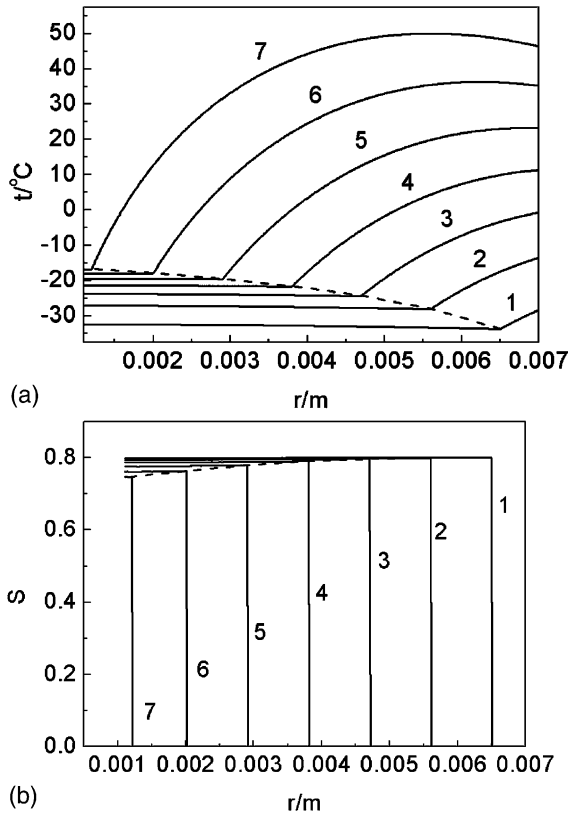

Fig. 3. (a) Temperature profiles during drying without a cylindrical dielectric core, (b) saturation profiles during drying without a cylindrical dielectric core, τ (s): 1—541; 2—1613; 3—2643; 4—3607; 5—4479; 6—5225; 7—5790 (sublimation front).

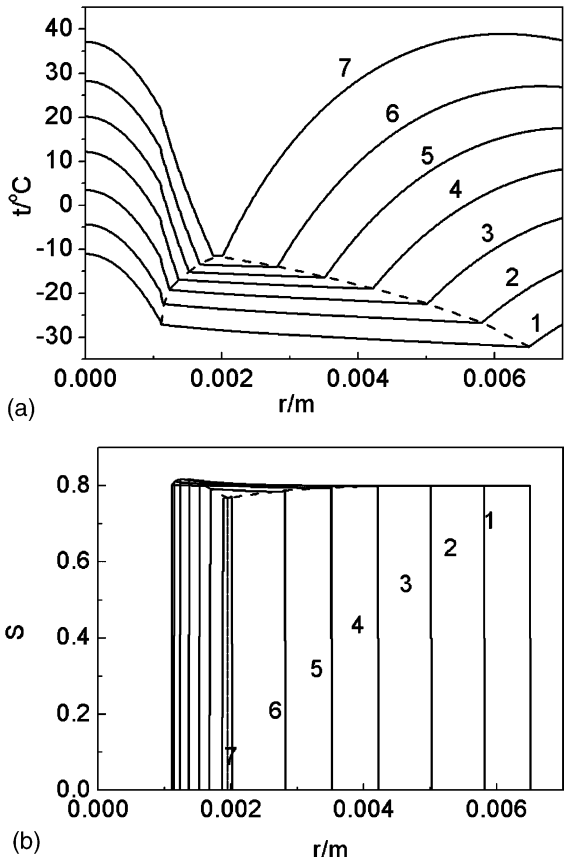

Fig. 4. (a) Temperature profiles during drying with a cylindrical dielectric core, (b) saturation profiles during drying with a cylindrical dielectric core, τ (s): 1—409; 2—1029; 3—1707; 4—2347; 5—2867; 6—3342; 7—3853 (sublimation front).

tribution in the material during drying is shown in Fig. 3(b). As seen on this figure, the saturation is almost unchanged during the initial phase. This is because of the fact that the temperature of the material is low and the sublimation is not apparent at this early stage.

As previously mentioned, the porous material with the cylindrical dielectric core would be heated from both inside and outside, one would expect two sublimation fronts exist. Fig. 4(a) shows the calculated temperature distribution in the cylindrical dielectric core and material during microwave freeze- drying at different time steps. The results in Fig. 4(a) clearly show that there do exist two sublimation fronts and they move gradually towards each other during the whole drying process. The abscissa in Fig. 4(a) is the distance from the cylindrical dielectric core center and the temperature distributions at different time, $\tau = 409$, 1029, 1707, 2347, 2867, 3342 and 3853 s are shown and marked 1, 2, 3, 4, 5, 6 and 7, respectively. These two sublimation fronts will finally meet at $r = 1.94$ mm and then the drying process be completed. There exists a change of temperature gradient at the position of the cylindrical dielectric core boundary, however, this can not be observed clearly because the chosen thermal conductivity difference between cylindrical dielectric core and material is relatively small. For the outer dried region, temperature gradient on the outer boundary indicates that the heat is initially absorbed from the environment to the material and then flows out to the environment. This result is almost identical to the previous result discussed in Fig. 3(a). Moreover, comparing the temperature curves with the curves presented in Fig. 3(a), it is obvious that the cylindrical dielectric core does have a significant effect on the drying rate. It should also be noted that, meanwhile, the local temperature in icy region is always below the triple point, which would guarantee no water appearance during the whole drying process.

The saturation distribution in the material at different drying times is depicted in Fig. 4(b). Curves 1–7 in Fig. 4(b) are the saturation distributions at $\tau = 409$, 1029, 1707, 2347, 2867, 3342 and 3853 s. In this study, 0.8 is taken as the initial moisture saturation. It

is interesting to note that local saturation near the second sublimation front could be higher than initial saturation during early stage of drying. This is because of the fact that vapor sublimated due to cylindrical dielectric core heating could not fully flow out of the icy region and is partly recondensed to be ice, which caused the increase of local saturation. This interesting phenomenon is clearly indicated by Fig. 4(b). This phenomenon will, however, disappear gradually with the decrease in saturation. The saturation distribution in icy region is flat. It can also be seen that the drying process is completed at the location of $r = 1.94$ mm, which consists with that of Fig. 4(a).

Fig. 5 shows the distributions of vapor density within porous media at different times during drying with a cylindrical dielectric core. The vapor density decreases monotonously from the cylindrical dielectric core boundary to the surface of the column during the entire drying process. Though the gradients are much larger in dried region, the vapor transfer exists in icy region as expressed in Eq. (9). Fig. 5 indicates that the vapor will be removed from icy region. As a result, the ice in icy region will sublimate and the saturation in this region will decrease as shown in Fig. 4(b). The vapor density curves in both dried region will also meet at the end of drying, as shown in curve 7.

The results presented in Fig. 6 show the variation of location of sublimation front with drying time. Comparison was done by calculating the position of sublimation front with cylindrical dielectric core and without, curves 2 and 1, respectively. The results shown in Fig. 6 correspond to those in Figs. 3 and 4. It is obvious that the drying curve for having cylindrical dielectric core case shows a dramatically increased drying rate. The drying curve plotted in Fig. 6 show that the cylindrical dielectric core case caused roughly half an hour reduction in drying time. This is explained by the fact that in the cylindrical dielectric core case, the material will be heated from both inside and outside. Thus, the temperature rise of the material will be accelerated and the heat provided for sublimation should also be increased accordingly. As a result, this situation results in a much higher drying rate. Therefore, the second sublimation front plays an important role in reducing drying time.

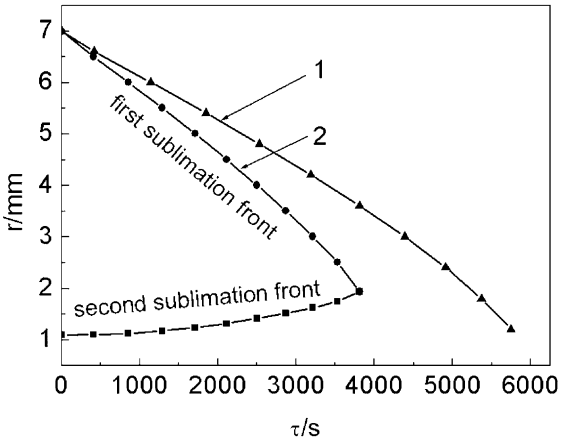

Fig. 6. The variation of location of sublimation fronts with drying time.

In Fig. 7, temperature curves at the moment of drying process termination are plotted for different initial saturations with cylindrical dielectric core. Four initial saturation conditions are used in the simulation i.e. $S = 0.2$, 0.4, 0.6 and 0.8. The abscissa in Fig. 7 is the distance from the cylindrical dielectric core center, and the initial radius of cylindrical porous material is kept constant as $R_p = 7.0$ mm. The temperature distributions at the end of drying, $\tau = 865$, 1826, 2826, and 3853 s are shown and marked 1, 2, 3, and 4, respectively. In each case, it is shown from the simulation results (Fig. 7) that

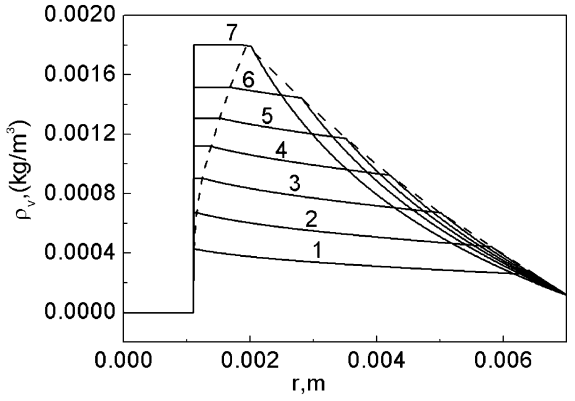

Fig. 5. Profiles of vapor density during drying with a cylindrical dielectric core, τ (s): 1—409; 2—1029; 3—1707; 4—2347; 5—2867; 6—3342; 7—3853 (sublimation front).

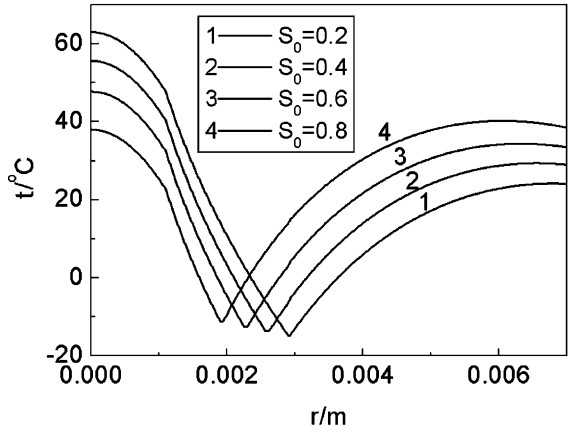

Fig. 7. Temperature curves at the moment of drying process termination for different initial saturations.

the shapes of the temperature distributions are similar at the end of drying, the main differences are due to different initial saturations. It is important to note that the end point of the second sublimation front is much closer to the outer layer of the material with the decrease of initial saturation. This is the result of higher temperature gradient and much more enhancive vapor transfer capability near the boundary of the cylindrical dielectric core, therefore, the moving velocity of the second sublimation front would be faster.

Fig. 8 demonstrates the variation of drying times for both cases at different initial saturations. The simulation model is used to study the effect of five different initial saturations on drying, i.e. $S = 0.2$, 0.4, 0.6, 0.8 and 1.0. Curves 1 and 2 of Fig. 8 represent drying under the conditions without and with cylindrical dielectric core heating. Numerical results have shown that the ratio of overall drying time of case 2–1 are 69.0%, 67.0%, 66.5%, 66.5% and 67.0%, respectively (see Table 3). Note also that the drying time is dramatically reduced from 21.0 to 14.4 min for the case at $S_0 = 0.2$ and from 122.3 to 82.0 min at $S_0 = 1.0$ when cylindrical dielectric core is applied. The effect of cylindrical dielectric core is clear. That is, when the initial saturation value is low ($S_0 = 0.2$), drying time is much changed. It, thus, could be concluded that for the constant microwave heating, it is expected that the cylindrical dielectric core should not be ignored even though initial saturation is low which is different from the spherical case as previously demonstrated [27]. This is because of the fact that the heat taken by vapor would flow out to the environment easily for cylindrical case. As a result, the temperature gradient would build up within the cylindrical dielectric core, and therefore, the impact of the second sublimation front produced by the dielectric core on drying time could not be ignored compared with that spherical case. For the operating conditions tested, it can be clearly seen that the drying times of both cases are nearly proportional to the initial saturation, which means that the drying time at any initial saturation can be predicted approximately by a linear relationship.

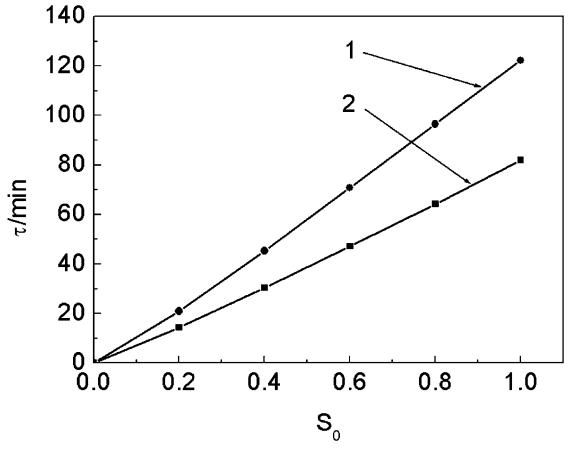

Fig. 8. The variation of drying times for both cases at different initial saturations: (1) without the cylindrical dielectric core; (2) with the cylindrical dielectric core.

The variation of drying times for both cases at different electric field strengths is illustrated in Fig. 9. The initial saturation S_0 is 0.8. A higher electric field strength causes higher energy input and in a shorter drying time. It should be noted that, however, too high an electric field strength might cause the accumulation of vapor locally and so the danger of local vapor pressure exceeding the triple point Ps.

Moreover, this figure also shows the reduction of the slope with the increase of electric field strength for the two cases, such a phenomenon can be observed apparently for the cylindrical dielectric core case. This indicates that too much higher electric field strength does not have a significant effect on drying time.

Fig. 10 shows the variation of drying time with the change of the loss factor of cylindrical dielectric core. The loss factor is an important parameter influencing the drying process. Under the operating conditions studied, four different loss factors, i.e. $\varepsilon'' = 2.0$, 3.0, 5.0 and 6.0, are investigated. Obviously, the bigger the loss factor, the shorter the drying time. A comparison shows that there is about 18.1 min difference in drying time between the two cases, $\varepsilon'' = 2.0$ and 6.0, the drying time are 82.3 and 64.2 min, respectively. Therefore, it is expected

Table 3
A comparison of overall drying times for different initial saturations

Initial saturation	Item		
	Drying time (min) (with the cylindrical dielectric core), τ_a	Drying time (min) (without the cylindrical dielectric core), τ_b	Drying time ratio, τ_a/τ_b (%)
0.2	14.4	21.0	69.0
0.4	30.4	45.3	67.0
0.6	47.1	70.8	66.5
0.8	64.2	96.5	66.5
1.0	82.0	122.3	67.0

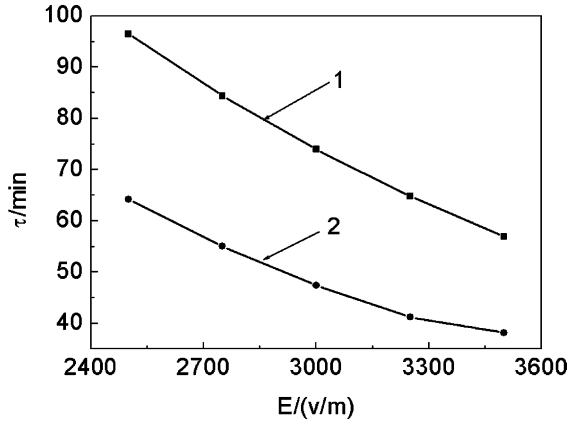

Fig. 9. The variation of drying times for both cases at different electric field strengths: (1) without the cylindrical dielectric core; (2) with the cylindrical dielectric core.

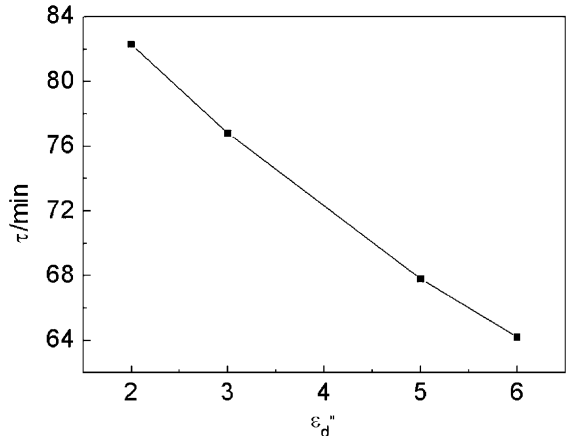

Fig. 10. The variation of drying time with the change of the loss factor of the cylindrical dielectric core.

that a moderate increase in loss factor of cylindrical dielectric core can result in a significantly shorter drying time. Also shown in Fig. 10, this plot suggests that the drying time is nearly inversely proportional to the cylindrical dielectric core loss factor. Moreover, much higher loss factor could lead to the melting of ice. This result may be attributed to the higher energy absorbed by the cylindrical dielectric core and the accumulative heat can not flow out to the environment easily.

Temperatures curves at the moment of drying process termination for different electric field strengths are plotted in Fig. 11. Calculations were done for four different electric field strengths: 2500, 2750, 3000 and 3250 V/m and the initial saturation is 0.8 (curves 1–4 in Fig. 11). Similar trends (V-bend) in the temperature distributions are obtained for each of the four cases. This figure also shows that the higher electric field strength results in the

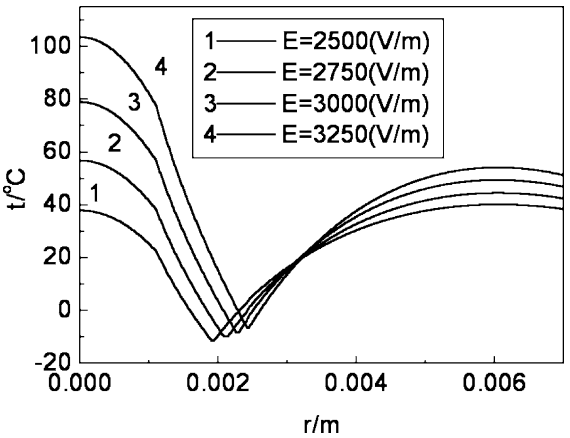

Fig. 11. Temperatures curves at the moment of drying process termination for different electric field strengths.

higher temperature gradient at the position of the cylindrical dielectric core boundary. High temperature gradient caused an increase of evaporating and increase of moving velocity of the second sublimation front. In the present study, the highest electric field strength $E = 3250$ V/m is used in the simulation. It is useful to note that the temperature within dried region can reach almost 80 °C. Such a result is due to the high level of the electric field strength employed. This situation may cause damage to the material quality.

Fig. 12 presents the drying time curves versus electric field strength for two different initial saturations, i.e. $S_0 = 0.4$ and 0.8. Cylindrical dielectric core was employed in this simulation. As previously discussed, the effect of electric field strength is apparent. The general trend for drying time variation is similar to that observed in Fig. 9. It is observed that, however, the reduction degrees of the slope presented in Fig. 12 are different during the process. Along with the increase of

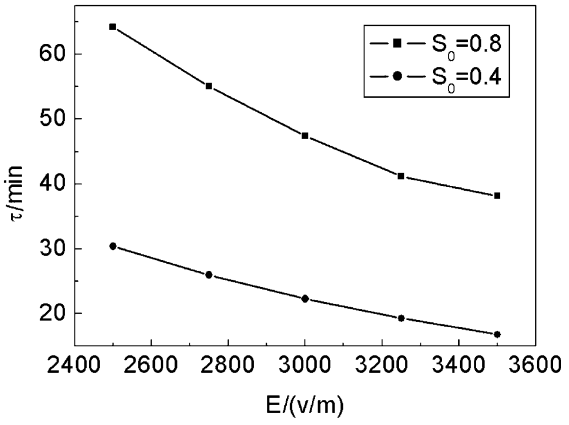

Fig. 12. Drying time curves versus electric field strength for two different initial saturations.

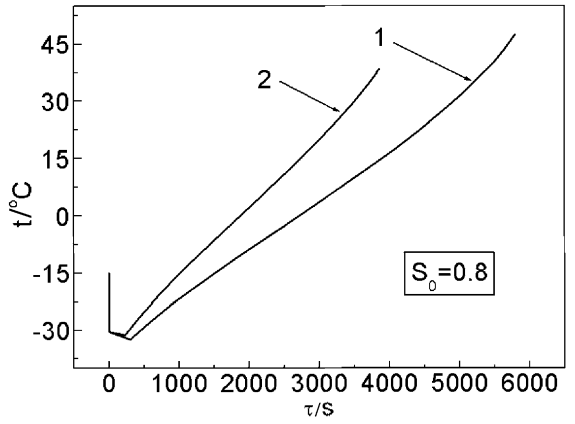

Fig. 13. The variations of surface temperature of cylindrical porous material: (1) without the cylindrical dielectric core; (2) with the cylindrical dielectric core.

electric field strength, the drying time in the high initial saturation case show a reduction much slower than in the low case. This means that lower initial saturation is of great advantage to drying under much higher electric field strength.

The variations of surface temperature of cylindrical porous material without and with the cylindrical dielectric core are shown in Fig. 13, curves 1 and 2, respectively. The ordinate is the surface temperature of porous material and the abscissa is drying time. For comparison purposes, the same initial saturation $S_0 = 0.8$ was selected. At the start of drying, because the sublimation front is much closer to the surface of the porous material, the evaporating resistance is small and the mass transfer driving force is high. However, the heat provided can not satisfy such high velocity of mass transfer. In both cases, therefore, the plot shows an initial rapid decrease in the temperature to a point where the heat transfer and mass transfer reach the equilibrium. From there till the end of the drying process, the temperature increases linearly. Also shown in Fig. 13, the surface temperature of the porous material is dried with the cylindrical dielectric core, relatively lower than that of without core at the end of drying. This is due to short drying time for the cylindrical dielectric core case.

5. Conclusions

The conjugate heat and mass transfer process within cylindrical porous media with cylindrical dielectric cores in microwave freeze-drying is investigated numerically. This study mainly concentrates on the influences of control parameters, such as loss factor, initial saturation and electric field strength, on microwave freeze-drying. Of the analysis of the results obtained it can be concluded that

- the loss factor ε'' of the cylindrical dielectric core is an important parameter influencing the drying process; a moderate increase in loss factor of cylindrical dielectric core can result in a much shorter drying time. Compared to spherical porous medium drying, cylindrical counterparts are much more dependent on the loss factor;
- the idea of two sublimation fronts originated for spherical porous media with spherical dielectric cores proved to be also applicable to cylindrical medium with cylindrical dielectric cores, and it could be generalized that the two sublimation front model should be successful in simulating porous media drying with dielectric cores, regardless of its structure form;
- numerical results show that the drying time is dramatically reduced from 21.0 to 14.4 min for the case at $S_0 = 0.2$ and from 122.3 to 82.0 min at $S_0 = 1.0$ when the cylindrical dielectric core is applied. This indicates that the cylindrical dielectric core should still be advised even though the initial saturation is low. This is different to the spherical case where the dielectric core is not necessary when the initial saturation is low. Under both cases, lower initial saturation condition results in shorter drying time;
- the intensity of electric field strength and the size of the cylindrical dielectric core should be well controlled during microwave freeze-drying in order to avoid ice melting. Moreover, a too high electric field strength does not have a significant effect on drying time. This phenomenon consists with the case of spherical ones.

References

[1] J. Flink, Energy analysis in dehydration processes, Food Technol. 31 (1977) 77–84.
[2] M.J. Pikal, S. Shah, D. Senior, J.E. Lang, Physical chemistry of freeze-drying: measurement of sublimation rates for frozen aqueous solutions by a microbalance technique, J. Pharm. Sci. 72 (6) (1983) 635–650.
[3] M.J. Millman, A.I. Liapis, J.M. Marchello, An analysis of the lyophilization process using a sorption–sublimation model and various operational policies, AIChE J. 31 (1985) 1594–1604.
[4] A.I. Liapis, R. Bruttini, Freeze drying, in: A.S. Mujumdar (Ed.), Handbook of Industrial Drying, Marcel Dekker, New York/Basel, 1995, pp. 309–343.
[5] A.I. Liapis, M.J. Pikal, R. Bruttini, Research and development needs and opportunities in freeze drying, Drying Technol. 14 (1996) 1265–1300.
[6] S. Jackson, S.L. Rickter, C.O. Chichester, Freeze drying of fruits, Food Technol. 11 (1957) 468–473.
[7] D.A. Copson, Microwave sublimation of foods, Food Technol. 12 (6) (1958) 270–272.
[8] M.W. Hoover, A. Markantonatos, W.N. Parker, Engineering aspects of using UHF dielectric heating to accelerate the freeze-drying of foods, Food Technol. 20 (6) (1966) 107–110.

[9] M.W. Hoover, A. Markantonatos, W.N. Parker, UHF dielectric heating in experimental acceleration of freeze-drying of foods, Food Technol. 20 (6) (1966) 103–107.
[10] Y.H. Ma, P. Peltre, Freeze dehydration by microwave energy: Part I. Theoretical investigation, AIChE J. 21 (2) (1975) 335–344.
[11] Y.H. Ma, P. Peltre, Freeze dehydration by microwave energy: Part II. Experimental investigation, AIChE J. 21 (2) (1975) 344–350.
[12] T.K. Ang, J.D. Ford, D.C.T. Pei, Microwave freeze-drying of food: a theoretical investigation, Int. J. Heat Mass Transfer 20 (5) (1977) 517–526.
[13] T.K. Ang, D.C.T. Pei, J.D. Ford, Microwave freeze-drying of food: an experimental investigation, Chem. Eng. Sci. 32 (1977) 1477–1489.
[14] J. Sochanske, J. Goyette, T. Bose, C. Akyel, R. Bosisio, Freeze dehydration of foamed milk by microwave, Drying Technol. 8 (1990) 1017–1037.
[15] J.W. Gould, E.M. Kenyon, Gas discharge and electric field strength in microwave freeze-drying, J. Microwave Power 6 (2) (1971) 151–167.
[16] T.K. Ang, J.D. Ford, D.C.T. Pei, Optimal modes of operation for microwave freeze drying of food, J. Food Sci. 43 (1978) 648–649.
[17] T.N. Chang, Y.H. Ma, Application of optimal control strategy to hybrid microwave and radiant freeze drying system, in: Drying 85, Hemisphere, Washington, DC, 1985, pp. 249–253.
[18] Y.H. Ma, P. Peltre, Mathematical simulation of a freeze drying process using microwave energy, in: Food PreservationAIChE Symposium Series, vol. 69, 1973, pp. 47–54.
[19] S.D. Chen, R.Y. Ofoli, E.P. Scott, J. Asmussen, Volatile retention in microwave freeze-dried model foods, J. Food Sci. 58 (1993) 1157–1161.
[20] M.H. Shi, Z.H. Wang, A sublimation–condensation theory for the microwave freeze drying of unsaturated porous media, J. Southeast Univ. (China) 25 (4) (1995) 92–98 (in Chinese).
[21] Z.H. Wang, M.H. Shi, Analysis of heat and mass transfer for microwave freeze drying of unsaturated porous media, J. Chem. Ind. Eng. (China) 47 (2) (1996) 131–136 (in Chinese).
[22] Z.H. Wang, M.H. Shi, Effects of heating methods on vacuum freeze drying, Drying Technol. 15 (5) (1997) 1475–1498.
[23] Z.H. Wang, M.H. Shi, Numerical study on sublimation–condensation phenomena during microwave freeze drying, Chem. Eng. Sci. 53 (18) (1998) 3189–3197.
[24] Z.H. Wang, M.H. Shi, Microwave freeze drying characteristics of beef, Drying Technol. 17 (3) (1999) 433–447.
[25] H.B. Arsem, Y.H. Ma, Aerosol formation during the microwave freeze dehydration of beef, Biotechnol. Progr. 1 (1985) 104–110.
[26] H.B. Arsem, Y.H. Ma, Simulation of a combined microwave and radiant freeze dryer, Drying Technol. 8 (1990) 993–1016.
[27] H.W. Wu, Z. Tao, G.H. Chen, H.W. Deng, Conjugate heat and mass transfer process within porous media with dielectric cores in microwave freeze drying, Chem. Eng. Sci. 59 (14) (2004) 2921–2928.
[28] C.J. King, Freeze-Drying of Foods, CRC Press, Cleveland, OH, 1971.
[29] S.A. Goldblith, L. Rey, W.W. Rothmayr, Freeze Drying and Advanced Food Technology, Academic Press, New York, 1975.
[30] J.D. Mellor, Fundamentals of Freeze-Drying, Academic Press, New York, 1978.
[31] S. Whitaker, A theory of drying in porous media, Adv. Heat Transfer 13 (1977) 119–203.
[32] S.M. Yang, Heat Transfer, second ed., Beijing, China, 1987.
[33] H.R. Perry, D. Green, J.O. Maloney, Perry's Chemical Engineering Handbook, sixth ed., McGraw-Hill, New York, 1992.
[34] J.C. Harper, Transport properties of gases in porous media at reduced pressures with reference to freeze-drying, AIChE J. 8 (3) (1962) 298–302.